mathematics

MDPI

Article

Research on Modeling and Control of Turbine-Driven Coaxial Boiler Feed Pump Speed Regulation System Based on an Improved BP-PID Algorithm

Ning Ma [1], Lei Liu [1], Yibo Tai [2], Bin Feng [3], Li Wang [3], Zhenyong Yang [1] and Laiqing Yan [2,*]

[1] North China Electric Power Research Institute Co., Ltd., Beijing 100045, China; maningncepu@163.com (N.M.); hotplanell@sina.com (L.L.); 13810286796@163.com (Z.Y.)
[2] School of Electric Power, Civil Engineering and Architecture, Shanxi University, Taiyuan 030006, China; 15525951892@163.com
[3] Xi'an Branch of North China Electric Power Research Institute Co., Ltd., Xi'an 710065, China; 13389187970@163.com (B.F.); wang15735044487@163.com (L.W.)
* Correspondence: yanlq@sxu.edu.cn

Abstract

The turbine-driven coaxial boiler feed pump (TD-BFP) speed regulation system is a core auxiliary machine in thermal power generating units. Its complex physical characteristics, including strong square-law nonlinearity, multivariable coupling, and large inertia, pose significant challenges for conventional fixed-parameter PID controllers, which often suffer from severe regulation lag, integral windup, and high-frequency oscillation during wide-range operating condition transitions. To address these issues, an improved adaptive PID control strategy based on a Back Propagation (BP) neural network is proposed in this paper. Specifically, to overcome the negative control gradient loss caused by the square-law resistance in the physical model, a sign-preserving mapping logic ($u \mid u \mid$) is innovatively designed. Furthermore, a dynamic anti-integral windup mechanism with physical boundary constraints and a first-order inertial filtering algorithm is introduced. Comprehensive simulation experiments on the Matlab/Simulink platform under high-load step operating conditions (3683 r/min and 1104 t/h) reveal that the proposed algorithm achieves millisecond-level, zero-overshoot tracking. Quantitative evaluations demonstrate that, compared with the traditional PID controller, the proposed method reduces the Root Mean Square Error (RMSE) by 88.29% and the Integral of Absolute Error (IAE) by 93.75%, achieving a near-perfect goodness of fit (R^2) of 0.9998. Additionally, the Total Variation (TV) of the control command is substantially decreased. These results convincingly demonstrate that the proposed controller perfectly balances extremely high dynamic fitting accuracy with reduced mechanical wear, presenting exceptional engineering application value for the localization transformation of power plant control systems.

Keywords: boiler feed pump; neural network control; adaptive PID; nonlinear dynamic modeling; sign-preserving mapping; anti-windup

MSC: 93C40; 93C10; 93C95

Check for updates

Academic Editor: Carlos Llopis-Albert

Received: 17 April 2026
Revised: 2 June 2026
Accepted: 5 June 2026
Published: 9 June 2026

Copyright: © 2026 by the authors. Licensee MDPI, Basel, Switzerland. This article is an open access article distributed under the terms and conditions of the Creative Commons Attribution (CC BY) license.

1. Introduction

With the large-scale integration of renewable energy into the power grid, modern thermal power generating units are frequently required to participate in deep peak shaving. Consequently, unit loads present characteristics of wide-range and rapid fluctuations [1].

As the "heart" of the thermal power plant, the turbine-driven coaxial boiler feed pump (TD-BFP) regulates the rotational speed through a hydraulic coupling to control the boiler feed water flow. This process encompasses both the rigid body dynamics of the mechanical rotor and the complex fluid dynamics of the water supply pipe network, making it a typical nonlinear, time-varying, and strongly coupled system [2].

In actual industrial sites, conventional Proportional–Integral–Derivative controllers are the most widely used algorithms due to their simple structure and ease of deployment [3]. However, because the pipe network resistance and pump head exhibit severe nonlinear square-law features ($H \propto \omega^2$), fixed-parameter PID controllers suffer from significant "parameter mismatch." When the unit experiences wide-range operating condition transitions, traditional PID controllers are highly prone to severe regulation lag, integral windup, and unacceptable overshoot [4]. To address these nonlinearities and external disturbances, Sliding Mode Control has been extensively studied. SMC forces the system states to slide along a predefined surface, providing excellent robustness against unmodeled dynamics and parameter variations [5]. Nevertheless, traditional first-order SMC suffers from the inherent "chattering" phenomenon caused by discontinuous switching functions. In the context of the TD-BFP system, such high-frequency chattering would lead to devastating mechanical wear and fatigue in the hydraulic coupling's scoop tube [6].

To mitigate the chattering problem while preserving robustness, Higher-Order Sliding Mode Control techniques, particularly the Super-Twisting Algorithm, have been proposed [7,8]. By hiding the discontinuous sign function under an integral term, HOSMC can provide continuous control signals and ensure finite-time convergence. Despite its mathematical elegance, HOSMC generally requires higher-order derivatives of the sliding variable or the design of complex extended state observers, making it highly sensitive to measurement noise in harsh power plant environments and difficult to implement in standard Distributed Control Systems [9].

Consequently, researchers have increasingly turned to intelligent and Adaptive Control strategies. Adaptive control mechanisms can dynamically update controller parameters to cope with time-varying system dynamics [10]. Fuzzy Logic Control is a prominent model-free adaptive approach that has been successfully applied to boiler and pump control systems [11,12]. By converting expert knowledge into fuzzy rules, FLC can effectively handle nonlinearities. However, the performance of FLC heavily relies on the accuracy of the predefined expert rule base, which is extremely difficult to construct and optimize for a newly retrofitted, wide-range coaxial BFP system.

Additionally, in the domain of intelligent control, fuzzy tracking control has been widely investigated to enhance the tracking performance of complex systems under uncertain operating conditions [13]. However, practical TD-BFP speed regulation systems are often subject to more severe physical constraints and degradation factors in industrial sites. On the one hand, typical actuator nonlinearities, such as dead-zone characteristics in hydraulic coupling control valves, usually degrade dynamic response speed and tracking accuracy, necessitating active dead-zone compensation strategies [14]. On the other hand, long-term harsh operations under high-load conditions are highly prone to internal leakage faults in the pump chambers, which dynamically alter the system parameters and degrade pump efficiency [15]. While traditional robust control or fixed fuzzy rules struggle to simultaneously adapt to these unmodeled faults and actuator nonlinearities without complex mathematical models, a learning-based adaptive approach, such as the proposed Back Propagation-Proportional-Integral-Derivative (BP-PID) BP-PID controller, provides a promising pathway to maintain stable regulation under such non-ideal physical states.

In recent years, Artificial Neural Networks have provided a powerful alternative for intelligent control [16]. Due to their universal approximation capabilities, NNs can

effectively learn unknown nonlinear mappings from input-output data. Among them, the Back Propagation neural network has been widely combined with PID control to form the BP-PID architecture [17]. By utilizing the backpropagation algorithm, the BP-NN can tune the K_p, K_i, and K_d parameters online in real time without requiring precise expert rules or complex mathematical observers.

Despite its theoretical advantages, directly applying the standard BP-PID algorithm to a fluid-mechanical system governed by square-law nonlinearities reveals critical flaws. Specifically, when a negative control error occurs (requiring deceleration), the negative sign of the control command is mathematically eliminated after passing through the physical square term (u^2). This converts a negative feedback command into a positive feedback disturbance, causing correct gradient-calculation directions to fail and leading to a "runaway" phenomenon [18]. Additionally, standard BP-PID lacks physical boundary awareness, making it susceptible to integral windup during high-load saturations.

This research is directly motivated by and conducted in support of the landmark project involving the localization modification of China's first steam turbine-driven coaxial boiler feedwater pump speed control system in 2025, which represents a critical milestone in securing the control autonomy and operational safety of large-scale thermal power units. Existing fixed-parameter or standard adaptive control methods either suffer from severe parameter mismatch during wide-range load transitions or risk control gradient loss and integral windup in highly nonlinear square-law systems. To address these issues, the proposed method specifically resolves the negative control gradient loss and actuator saturation windup during rapid deep peak regulation. Unlike conventional approaches that rely on complex, noise-sensitive mathematical models or standard unconstrained neural networks, the core difference in our method lies in integrating a physical-prior-constrained sign-preserving mapping logic and a dynamic anti-windup mechanism directly into the BP-PID framework. This integration guarantees both transient stability and rapid error recovery without requiring tedious on-site manual tuning.

To break through these bottlenecks, this paper proposes an improved adaptive BP-PID control strategy tailored for the TD-BFP system. The main contributions of this paper are summarized as follows:

(1) A sign-preserving mapping logic ($u \mid u \mid$) is innovatively designed and integrated with a priori Jacobian constraints to completely solve the negative control gradient loss problem in square-law physical models.
(2) A dynamic anti-integral windup mechanism based on physical boundary constraints is proposed, which dynamically freezes the integral gain during actuator saturation to achieve zero-delay recovery.
(3) A first-order dynamic inertial digital filter is introduced to effectively suppress the high-frequency oscillation of the control variables, thereby minimizing mechanical wear.

The rest of this paper is organized as follows: Section 2 establishes the comprehensive nonlinear fluid-mechanical coupled mathematical model of the TD-BFP system. Section 3 details the design and improvements of the proposed BP-PID controller. Section 4 presents the simulation experiments, comparative studies, and quantitative evaluations. Finally, the main conclusions are drawn in Section 5.

2. Dynamic Mathematical Modeling of the TD-BFP System

This paper decomposes the BFP system into two parts: the "mechanical rotation subsystem" and the "fluid dynamic subsystem" to establish differential equation models (Figures 1 and 2).

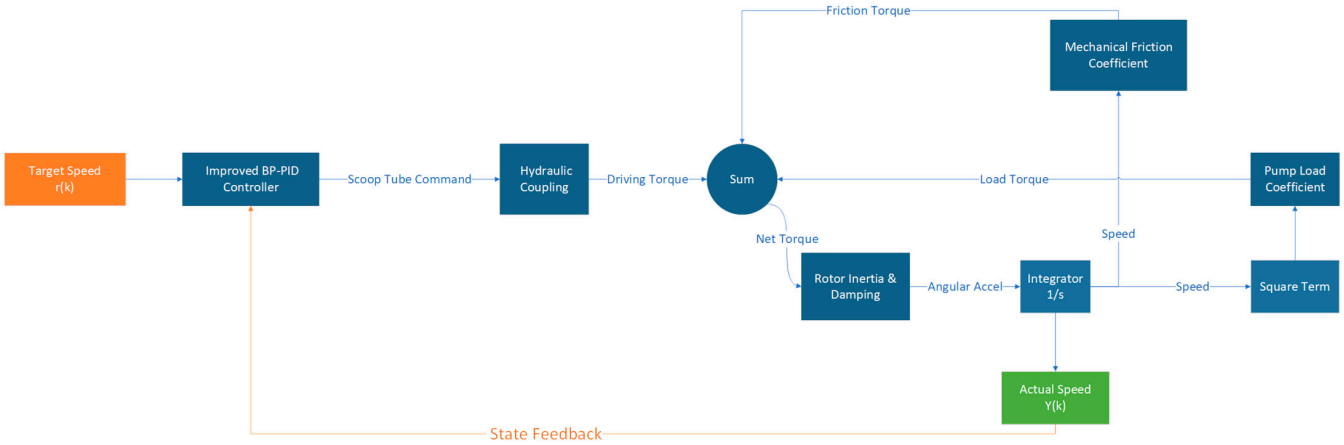


Figure 1. Schematic Diagram of the Mechanical Rotating Subsystem.

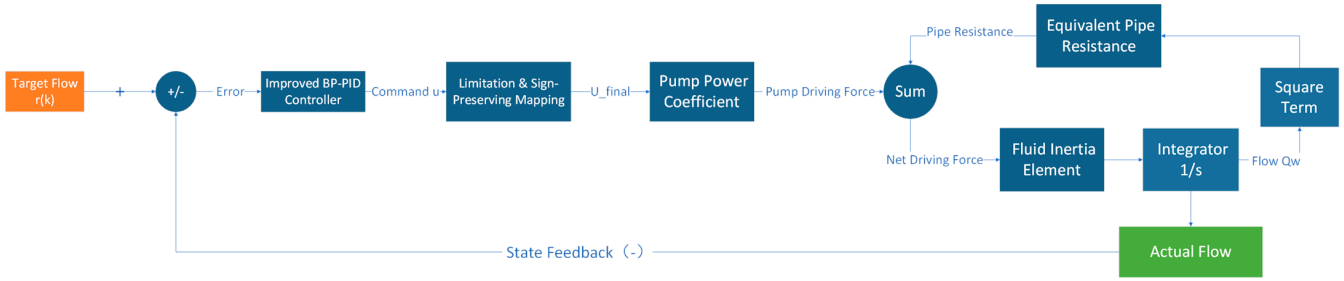


Figure 2. Schematic Diagram of the Hydraulic Subsystem.

2.1. Mechanical Rotation Subsystem Modeling

It should provide a concise and precise description of the experimental results, their interpretation, and the experimental conclusions that can be drawn.

The BFP is driven by a small steam turbine through a hydraulic coupling. According to rotor dynamics and Newton's second law, the mechanical motion equation of the shaft system can be expressed as:

$$J\frac{dw}{dt} = T_{drive} - T_{friction} - T_{pump} \tag{1}$$

where J is the equivalent rotational inertia of the unit shaft system (kg·m^2); w is the real-time speed of the BFP (rad/s); $T_{friction}$ is the mechanical friction and windage resistance torque, usually linearly related to the speed, i.e., $T_{friction}$; T_{pump} is the hydraulic load torque of the pump.

It is worth noting that T_{drive} is the driving torque transmitted by the hydraulic coupling, whose magnitude depends on the scoop tube opening command (the system input variable u) and the input-output slip, which can be approximately equivalent to:

$$T_{drive} = K_{oil} \cdot u \cdot (w_{in} - w) \tag{2}$$

where K_{oil} the coupling transmission gain, and w_{in} is the rated speed of the prime mover.

2.2. Fluid Dynamic Subsystem Modeling

The water pump converts mechanical energy into the pressure and kinetic energy of the fluid. According to pump affinity laws and fluid dynamics, the output head of the pump is directly proportional to the square of the rotational speed ($H_{pump} = k_{pump} \cdot \omega^2$).

Simultaneously, in the water supply pipe network, the resistance pressure drop is proportional to the square of the feed water flow rate ($H_{res} = k_{res} \cdot Q_w^2$). According to the

momentum equation for the fluid network, the rate of change in the pipeline fluid's momentum is driven by the pressure difference. Its differential equation can be expressed as:

$$\Gamma \frac{dQ_w}{dt} = H_{pump} - H_{res} = k_{pump} \cdot w^2 - k_{res} \cdot Q_w^2 \tag{3}$$

where $\boldsymbol{\Gamma}$ is the fluid inertia time constant, which is determined by the pipe length L, cross-sectional area $\boldsymbol{S}$, and fluid density $\boldsymbol{\rho_w}$ ($\boldsymbol{\Gamma = \rho_w L/S}$). As can be seen from Equations (1) to (3), there is a severe nonlinear coupling relationship between the speed $\boldsymbol{w}$ and the flow rate $\boldsymbol{Q_w}$.

3. Design of the Improved BP-PID Controller

While standard BP-PID is an established control strategy, its direct application to the TD-BFP system reveals significant limitations due to the severe square-law nonlinearities and physical actuator boundaries. Therefore, the actual contribution of this section is the development of a tailored control architecture that integrates sign-preserving mapping and bounded anti-windup logic into the BP-PID framework.

The target implementation platform for the proposed algorithm is a standard industrial Distributed Control System executing under IEC 61131-3 standards [19]. To facilitate real-time execution on embedded processors with limited computational resources, the optimization procedure relies on an online gradient descent method rather than computationally heavy predictive solvers. The detailed execution architecture and optimization procedure are illustrated in the flowchart in Figure 3. The flowchart demonstrates the sequential integration of input normalization, feedforward neural computation, anti-windup PID calculation, and backward propagation gradient updates constrained by physical prior knowledge.

3.1. BP Neural Network Topology and Forward Computation

A three-layer feedforward neural network of "input layer-hidden layer-output layer" is adopted. The network input is a four-dimensional vector $X = [r_{norm}, y_{norm}, e_{norm}]$ where $r_{norm}, y_{norm}, e_{norm}$ are the strictly normalized target setting value, system actual output value, and real-time error, respectively.

Both the hidden layer and the output layer use the Sigmoid activation function $f(x) = 1/(1 + e^{-x})$. The three nodes of the output layer correspond to the dimensionless bases $O_j^3 \in (0, 1)$ of the PID parameters. After mapping with the system static base value and the global amplification factor, the real-time tuned PID parameters are obtained:

$$\begin{cases} K_p(k) = K_{p0} + O_1^{(3)} \cdot Scal\ e_p \\ K_i(k) = K_{i0} + O_2^{(3)} \cdot Scal\ e_i \\ K_d(k) = K_{d0} + O_3^{(3)} \cdot Scal\ e_d \end{cases} \tag{4}$$

It is worth noting that the proposed BP neural network does not require offline pre-training and is fully updated online. In industrial applications, obtaining extensive and decoupled offline training datasets for the TD-BFP system is highly challenging. Therefore, the network weights are initialized with randomized small values, and the controller is "cold-started" by aligning it with a pre-calculated physical equilibrium point (u_1).

To prevent the neural network from generating unrealistic or extreme PID parameters during the online adaptive process, a strict mathematical bounding mechanism is designed. As shown in Equation (7), the raw outputs of the neural network are first strictly confined to the dimensionless interval (0,1) by the Sigmoid activation function. Subsequently, these values are mapped into safe, predefined engineering boundaries using the static base values (K_{p0}, K_{i0}, K_{d0}) and the global scaling factor ($Scale$). Furthermore, a hard saturation limit

is applied to the final calculated K_p, K_i, and K_d to ensure they never exceed the physical limits or become negative. This bounding logic mathematically guarantees the Bounded-Input–Bounded-Output (BIBO) stability of the controller, completely eliminating the risk of system divergence caused by weight explosion during online learning.

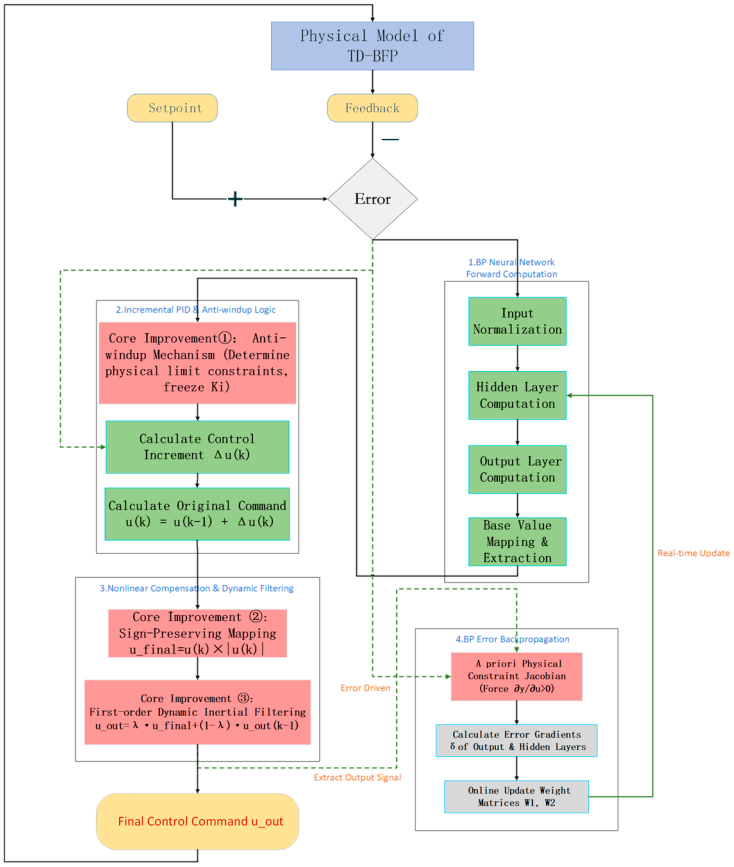


Figure 3. Internal logic control flow chart of the improved BP-PID controller.

3.2. Incremental PID and Physical Boundary Anti-Windup Logic

The controller calculates the command increment Δu using the incremental PID control law:

$$\Delta u = K_p(k)[e(k) - e(k-1)] + K_i(k)e(k) + K_d(k)[e(k) - 2e(k-1) + e(k-2)] \quad (5)$$

To prevent the system from hitting the safe upper and lower limits of the physical actuator during the startup phase or large step disturbances, conditional judgment logic is introduced:

$$K_i(k) = \begin{cases} 0, & if(u(k-1) \geq U_{max} \wedge e(k) > 0) \vee (u(k-1) \leq U_{min} \wedge e(k) < 0) \\ K_i(k) & otherwise \end{cases} \quad (6)$$

This anti-windup logic avoids integral storms and greatly shortens the recovery time of the system exiting the restricted area.

The conditional disabling of the integral gain K_i during the physical saturation state does not compromise system stability; rather, it is a critical measure to preserve transient stability. When the control command hits the absolute physical boundaries of the actuator (e.g., the maximum speed limit of 3500 r/min), the actuator cannot execute any further increase in the command. If the integral action remains active under such conditions, the sustained error will cause massive "phantom" accumulation (Integral Windup).

Consequently, when the target setpoint decreases, the system would exhibit a severe phase lag and hazardous overshoot due to the time required to "unwind" the inflated integral term.

By temporarily freezing K_i under the dual conditions of "hitting the boundary" and "the error direction driving further into saturation", the accumulation of invalid errors is thoroughly cut off. During this freezing period, the proportional K_p and derivative (K_d) terms remain fully active. This ensures that the moment the target error reverses, the controller instantly outputs a restorative command, allowing the system to exit the saturation region with zero delay. Therefore, this anti-windup mechanism significantly enhances the dynamic stability and robustness of the highly nonlinear hydraulic system under extreme load disturbances.

3.3. Sign-Preserving Mapping ($u|u|$) and Backpropagation Constraints

The traditional algorithms, when a negative error (requiring deceleration) is output, the negative sign is eliminated after passing directly through the square loop u^2, converting it into a positive acceleration command, resulting in a "runaway" phenomenon. This paper proposes improving the conventional square mapping to a sign-preserving mapping:

$$u_{final} = u(k) \cdot |u(k)| \tag{7}$$

Simultaneously, when calculating the output layer gradient $\delta_j^{(3)}$ via BP network backpropagation, prior physical knowledge is used to forcibly constrain the control gradient direction $\frac{\partial y}{\partial u} > 0$:

$$\delta_j^{(3)} = e(k) \cdot \frac{\partial y}{\partial u} \cdot \frac{\partial u}{\partial O_j^{(3)}} \tag{8}$$

These two measures combined completely eliminate the hidden danger of reverse erroneous learning in neural networks in square-law nonlinear systems.

3.4. Dynamic Inertial Digital Filtering

Since high-frequency industrial data inherently contains noise, a high-gain BP-PID is highly susceptible to high-frequency oscillation. To address this, a standard first-order inertial digital filter is applied to the controller's output end. By rationally setting the filter's smoothing coefficient, the action command of the control valve is smoothed without sacrificing system response speed, thereby effectively reducing mechanical wear.

3.5. Quantitative Evaluation Metric System for Control Performance

To objectively evaluate the tracking accuracy and robustness, four classical comprehensive performance evaluation metrics are introduced: Root Mean Square Error (RMSE), Mean Absolute Error (MAE), Integral of Absolute Error (IAE), and Coefficient of Determination (R^2).

$$RMS = \sqrt{\frac{1}{N}\sum_{i=1}^{N}(r(i) - y(i))^2} \tag{9}$$

$$MAE = \frac{1}{N}\sum_{i=1}^{N}|r(i) - y(i)| \tag{10}$$

$$IAE = \sum_{i=1}^{N}|r(i) - y(i)| \cdot \Delta t \tag{11}$$

$$R^2 = 1 - \frac{\sum_{i=1}^{N}(r(i) - y(i))^2}{\sum_{i=1}^{N}(r(i) - r)^2} \tag{12}$$

$$ISE = \sum_{i=1}^{N} e(i)^2 \cdot \Delta t \tag{13}$$

$$ITAE = \sum_{i=1}^{N} t(i) \cdot \mid e(i) \mid \cdot \Delta t \tag{14}$$

4. Simulation Experiments and Result Analysis

In order to verify the engineering applicability and superiority of the improved BP-PID algorithm proposed in the domestic speed control transformation of large thermal power unit coaxial water pumps, a high-fidelity fluid-mechanical coupling digital twin model was built in the Matlab/Simulink (version R2023b) environment, and a closed-loop simulation test was carried out.

It should be emphasized that all performance data and transient response curves presented for the "Improved BP-PID" in these comparative studies are obtained by applying the latest, fully optimized version of our algorithm as detailed in Section 3. The baseline models, including the traditional fixed-parameter PID and the conventional Sliding Mode Control (SMC), are evaluated under identical operating profiles to clearly demonstrate the specific improvements. This comparative analysis highlights how the newly designed sign-preserving mapping, dynamic anti-windup logic, and dynamic filtering directly translate into superior performance metrics under both steady-state and wide-range transient conditions.

To highlight the comprehensive advantages of improving algorithms, this paper sets up a double comparison baseline: it not only introduces the traditional fixed parameter PID controller based on engineering experience rectification as a basic reference, but also introduces the conventional sliding mode controller (SMC) recognized as having strong anti-interference ability in the nonlinear control field as an advanced comparison and reference.

4.1. Simulation Parameter Settings

Actual operating data during a certain period were extracted as the target reference. The test condition focuses on the high-load region, where the speed target value is approximately 3683 rad/s, and the corresponding flow rate is approximately 1104 m^3/h. The physical parameters of the model are set to J = 10, $k_{pump} = 0.00925$, $k_{res} = 0.005$.

The controller parameters are set as follows: learning rate $\eta = 0.0001$, inertial coefficient $\alpha = 0.05$, and global scaling factor System Scale = 60.0. To achieve a bumpless startup, the initial equilibrium point of the controller is precisely aligned to $u_1 = 2609.8$.

4.2. Comparison and Analysis of Dynamic Tracking Characteristics Under Different Operating Conditions

To comprehensively evaluate the dynamic tracking ability of the algorithm in the nonlinear time-varying system, this section intercepts typical characteristic sections such as global steady state, wide-range step mutation, and deep negative regulation for local amplification and mechanism analysis.

4.2.1. Global Tracking Performance and Steady-State Analysis

To comprehensively evaluate the long-term stability and adaptation of the proposed algorithm under dynamic operating conditions, a continuous simulation test spanning tens of thousands of seconds was executed. The global tracking performance of the three controllers under varying load demands is illustrated in Figure 4. In the following subsections, the detailed performance is analyzed under steady-state, step-change, and rapid-deceleration scenarios.

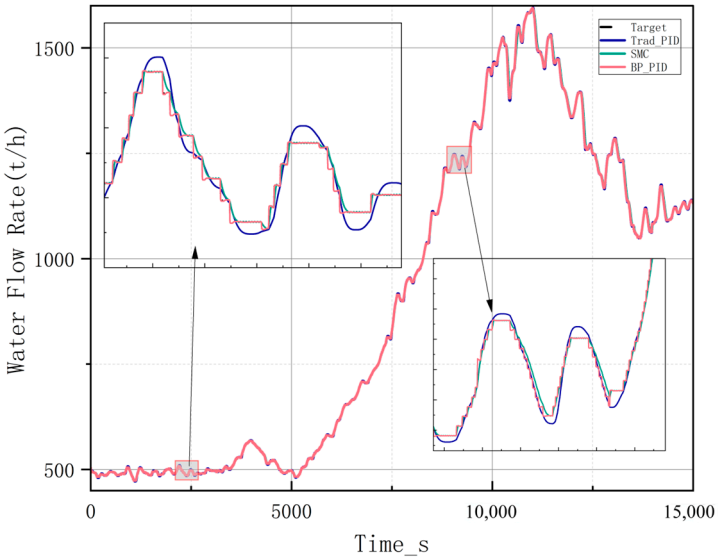


Figure 4. Comparison of Global Tracking Performance Among Different Control Algorithms Under Changing Operating Conditions.

As shown in Figure 4, in the complex condition test with tens of thousands of seconds and a large flow span, the three control algorithms show completely different global steady-state characteristics. Due to the fixed gain, the traditional PID controller is completely unable to adapt to the quadratic nonlinear damping mutation caused by the increase in pipeline network traffic and shows obvious tracking delay and low-frequency oscillation in the global range.

In contrast, both the conventional SMC algorithm and the improved BP-PID algorithm proposed in this paper have shown strong robustness and can closely match the target set value. However, it can be observed in the local magnification that the SMC algorithm is accompanied by fine high-frequency jitter in the steady-state maintenance region, while the curve of the improved BP-PID algorithm is the smoothest, and the steady-state error is almost zero.

4.2.2. Analysis of Wide-Range Step-Change Tracking Capability

To evaluate the rapid response and dynamic tracking capability of the controllers during load mutations, a sequence of step-change instructions was introduced. The local dynamic tracking curves under these wide-range step mutations are compared in Figure 5.

When the water supply pump system participates in the primary FM of the power grid, it often faces a stepped jump with dense load instructions. For example, when the water supply pump system participates in the depth peak adjustment of the power grid, it often faces a stepped jump with dense load instructions. As shown in Figure 5, when the target flow rises sharply, the traditional PID is limited by a fixed proportional gain and cannot overcome the large inertial delay, resulting in obvious response delay and wave peak overtuning. Conventional SMC algorithms rely on nonlinear switching terms to quickly keep up with the jump, but are limited by the length of walking; there is an inevitable penetration overtuning at the corner of the ladder.

The improved BP-PID controller mentioned in this paper uses the transient strong thrust calculated forward by the neural network to have a strong proportional adjustment effect at the moment of jumping, realizing the "zero delay" bite of the ladder jump rising edge; at the same time, through dynamic integral adjustment, the over-modulation phenomenon is completely eliminated, showing the most Excellent dynamic agility.

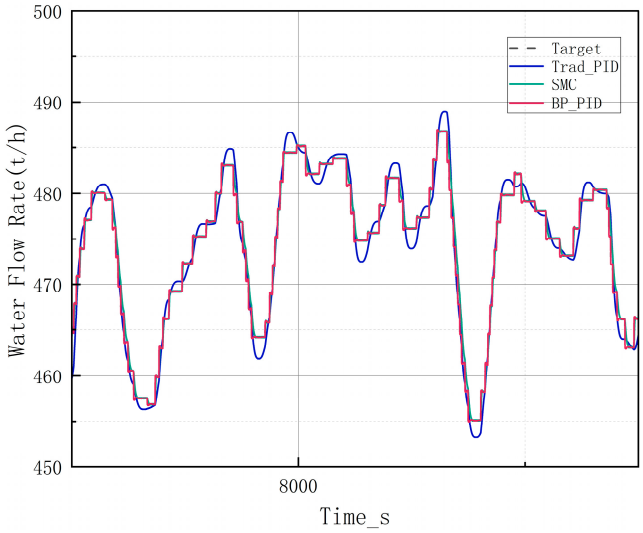


Figure 5. Comparison of Local Dynamic Tracking Under Wide-Range Step-Change Conditions.

4.2.3. Analysis of Negative Deep Regulation and Anti-Integral Windup Characteristics

The negative depth modulation and rapid current reduction tests were conducted to evaluate the controllers' behavior under strong nonlinear reverse gradients. The comparative tracking performance and corresponding anti-integral saturation characteristics are presented in Figure 6.

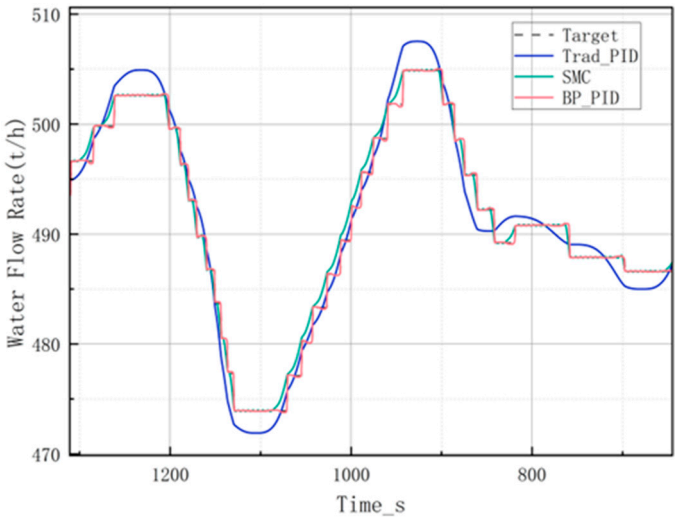


Figure 6. Comparison of Negative Depth Modulation and Anti-Integral Saturation Characteristics.

Due to the nonlinear characteristics of the square term (Q_w^2) of the fluid resistance of the pipeline network, the system is very easy to lose negative control force when performing the task of rapid current reduction. As shown in the deep fall zone shown in Figure 6, the traditional PID controller loses the negative control gradient, coupled with the serious Integral Windup, causing the flow curve to hover at a high level when the target dives and cannot fall back. Under this extreme condition, both SMC and the improved BP-PID have successfully achieved a quick U-turn. In particular, the improved BP-PID algorithm, thanks to the strong intervention of the symbol retention mapping and anti-integration saturation dynamic freezing logic designed in this paper, opens up the negative conduction channel while cutting off the invalid integral. Its descending trajectory is smoother than SMC, which perfectly verifies the algorithm under asymmetric load conditions. Extreme robustness is achieved.

To evaluate the transient behavior under extreme reverse regulation and quantitatively substantiate the contribution of the proposed dynamic anti-integral windup mechanism, an ablation study was carried out [15]. We compared the proposed adaptive controller (Anti-Saturation-BP) with an ablated version (Non-Anti-saturation-BP), where the conditional freezing logic of the integral gain K_i was deactivated. The comparative tracking performance under a rapid setpoint step-down mutation is illustrated in Figure 7.

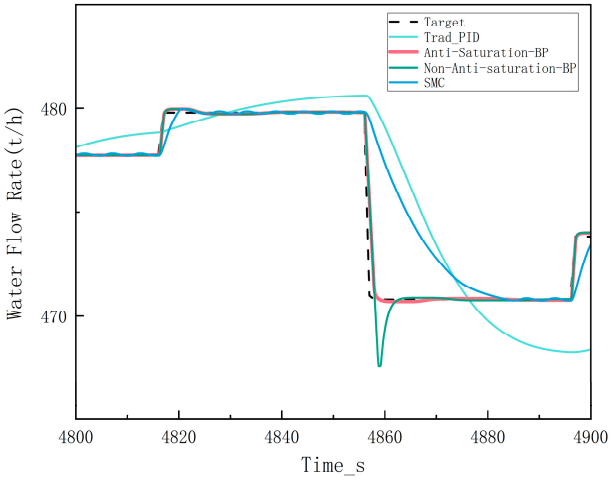


Figure 7. Comparative dynamic tracking curves and ablation study of the anti-integral windup mechanism during a rapid step-down mutation.

As shown in Figure 7, at $t = 4856$ s, the target water flow rate undergoes a sharp downward step-change from 480 t/h to 471 t/h, representing a step amplitude of 9 t/h. Under this rapid transition, the proposed Anti-Saturation-BP controller exhibits highly agile and stable tracking, utilizing the conditional freezing logic of K_i to prevent invalid integral state accumulation during the preceding saturated high-load phase. Consequently, at the instant of setpoint reversal, the proposed controller reacts almost zero-delay, tracking the target down to exactly 471 t/h with a recovery settling time of less than 1.0 s and no noticeable transient undershoot. In contrast, the ablated Non-Anti-saturation-BP controller drops abruptly but suffers from a significant transient undershoot, plunging to a minimum of 468.2 t/h. This transient deviation corresponds to a dynamic undershoot of approximately 31.1% of the step amplitude and requires a settling recovery delay of approximately 6.0 s to return to the stable reference, which is a direct consequence of the accumulated saturated integral states failing to unwind immediately upon error reversal. Furthermore, the baseline traditional PID and SMC controllers both exhibit severe sluggishness with substantial phase lags, requiring more than 30 s and 20 s, respectively, to decay to the new target. These consolidated results demonstrate that the proposed dynamic anti-windup mechanism is mathematically and physically necessary to mitigate the adverse effects of actuator saturation, thereby ensuring dynamic transient agility and system stability.

4.2.4. Validation and Analysis of Wide-Range Variable Condition Robustness

To further investigate the control precision and robustness under wide-range large-scale operating variations, a multi-stage step-down and step-up sequence was implemented. Figure 7 displays the global tracking performance and local magnification of the three controllers.

The smoothness of the control instruction directly determines the mechanical wear life and operation safety of the water supply pump adjustment mechanism. As shown in the local magnification area in Figure 7, the equivalent control output instructions of the three algorithms show essential differences.

In order to forcibly eliminate system errors, the output instructions of traditional PID produce a large amount of low-frequency dissipation oscillation. As a representative of nonlinear robust control, the SMC algorithm performs well in flow tracking, but its switching characteristics based on discontinuous symbol functions trigger extremely serious high-frequency vibration, and the equivalent control signal twitches violently in a very short time. If this extreme control output directly acts on the physical actuator, it will cause devastating mechanical fatigue and structural damage. In contrast, the improved BP-PID algorithm proposed in this paper strictly converges the control instructions in a very small fine-tuning interval through the attenuation effect of the first-order dynamic inertial digital filter and the flexible suppression of the weight of the neural network. This result strongly proves that the improvement of the BP-PID algorithm not only fundamentally overcomes the tremor-intractable disease of SMC but also effectively avoids the ups and downs of traditional PID, showing a high "mechanical friendliness" for physical devices.

In the full-time wide-range load migration, the improved BP-PID algorithm realizes the close tracking coverage of the target set value. Through local feature extraction, the dynamic differences between the three control algorithms in different nonlinear intervals can be clearly observed:

(1) Robust analysis of the low-load area

When the unit load is lowered from 1100 t/h to 500 t/h, the system fluid damping decays rapidly. At this time, the traditional fixed-parameter PID controller based on high-load rectification has a serious "parameter mismatch", which is manifested as continuous low-frequency large oscillations that cannot stabilize the flow. Although conventional sliding mode control can forcibly bite the target with the nonlinear convergence law, it causes violent high-frequency vibration under low-damping conditions. With the powerful generalization and adaptive optimization ability of the neural network, the improved BP-PID has independently completed the parameter reconstruction of kp and ki and still maintains smooth and accurate tracking without static difference under the new low-load conditions.

(2) High-load step tracking analysis

When the system load suddenly increases and is accompanied by dense step-shaped instruction jumps, the traditional PID is limited by a fixed proportional gain and cannot overcome the large inertial lag. There is an obvious slow response and wave peak overmonization at each rising edge and falling edge. Although the conventional SMC algorithm responds extremely fast, it is limited by discontinuous switching gain, inevitably leading to penetrating overtuning and high-frequency jitter occurring at the corner of the ladder. In contrast, the improved BP-PID uses a transient strong thrust to quickly bite the target at the moment of jump, and effectively suppresses burrs through first-order dynamic filtering in the steady state, achieving the perfect response of "no overtuning and zero delay.

In summary, the wide-range dynamic test of this group fully proves that compared with the poor adaptability of traditional linear PID and the vibration defects of conventional nonlinear SMC, the control strategy proposed in this paper can perfectly overcome the strong nonlinearity and time variability of the hydrodynamic system without tedious on-site segmentation and rectification, and has extremely high adaptability to full working conditions. Competency and safety of the executive body.

4.3. Analysis of Actuator Control Command Smoothness

Smooth and continuous control signals are crucial for extending the service life of hydraulic valves and coupling actuators. The equivalent control drive commands output by the three controllers are compared in Figure 8.

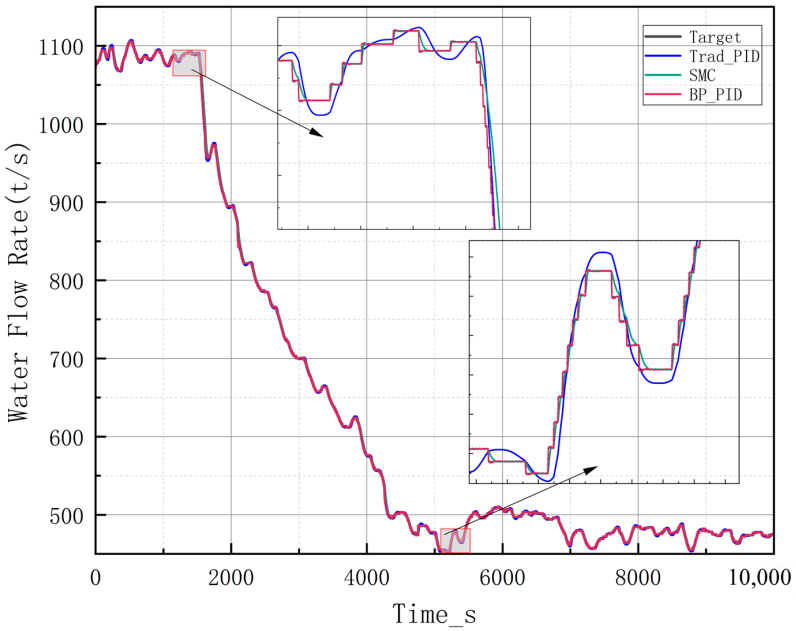


Figure 8. Comparison of Global Tracking and Robustness Among Different Control Algorithms Under Wide-Range, Large-Scale, and Variable Operating Conditions.

Comparing the equivalent output instructions of the three control algorithms, it can be seen that when facing large-span changes, the traditional PID produces violent fluctuations for a long period; while the conventional sliding mode control can respond quickly, it is limited by discontinuous switching gain, resulting in extremely serious high-frequency vibration, as shown in the green curve of Figure 8. If this high-frequency oscillation directly acts on the hydraulic coupler, it can easily cause fatigue damage to the mechanical actuator.

In contrast, the improved BP-PID algorithm proposed in this paper ensures extremely-fast tracking speed while the output instructions are extremely smooth. This not only fundamentally overcomes the intractable problem of SMC but also effectively avoids the ups and downs of traditional PID, showing the high 'mechanical friendliness' and safety and security value for the physical equipment of the water supply pump (Figure 9).

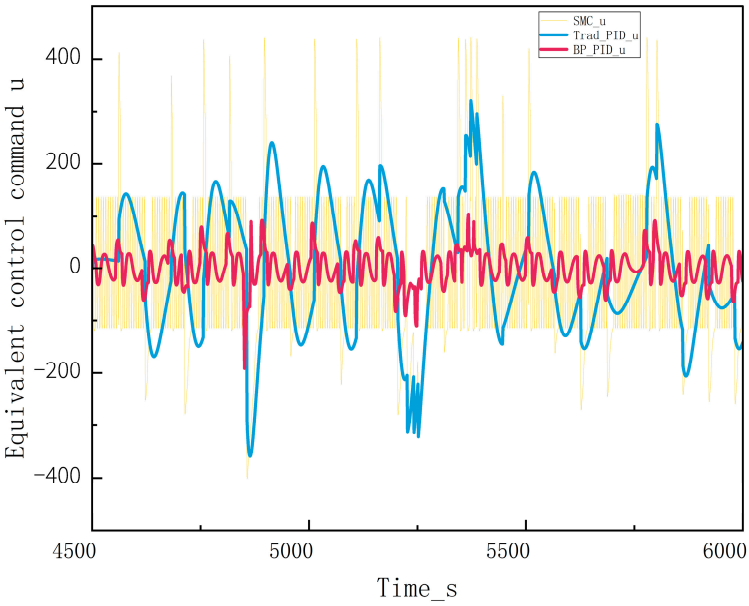


Figure 9. Comparison of the Dynamic Characteristics of Equivalent Drive Commands Output by the Controller.

4.4. Online Adaptive Evolution Mechanism of BP Neural Network Parameters

To reveal the internal "white-box" mechanism of the improved algorithm in achieving high-frequency, precise tracking, the online tuning trajectories of PID parameters in complex disturbance intervals are extracted. It can be clearly observed that the neural network does not output static constant values, but relies on real-time error (e) and Jacobian gradients, demonstrating extremely strong "bionic thinking" capabilities: At the moment the set value jumps, the network rapidly pulls up the proportional gain Kp to provide transient strong driving force; when the actual output approaches the target value and enters the steady-state region, Kp drops rapidly to prevent overshoot, while the integral gain Ki undergoes high-frequency flexible fine-tuning to smooth out extremely small steady-state errors. This dynamic evolution trajectory fully proves that the BP network can achieve the global optimal configuration of the underlying control law through continuous environmental interaction (Figure 10).

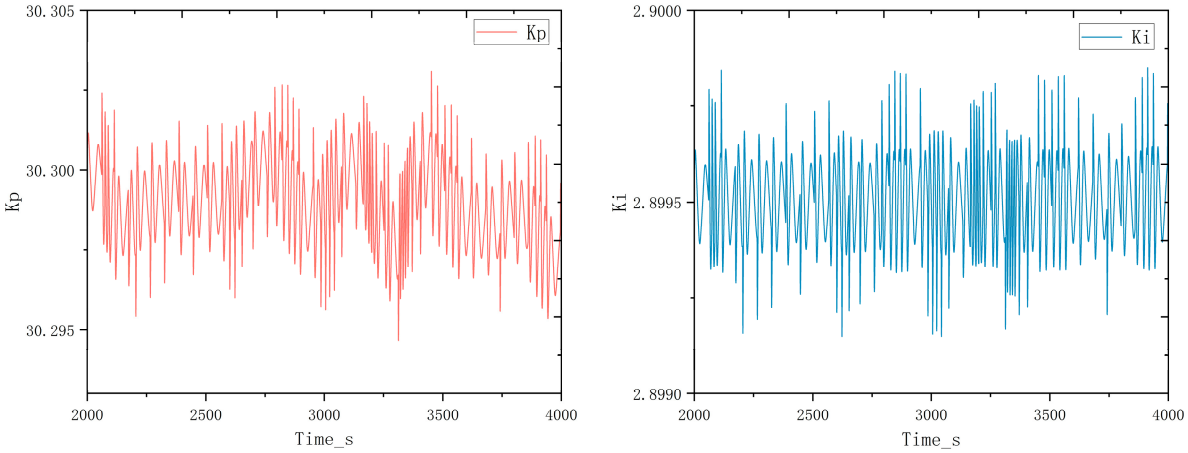


Figure 10. Online adaptive tuning trajectory of PID gain parameters using a BP neural network: (**a**) Dynamic evolution trajectory of the proportional gain Kp; (**b**) Dynamic evolution trajectory of the integral gain Ki.

To evaluate the sensitivity of the proposed controller to the training parameters, key hyperparameters including the learning rate η and the inertial coefficient α were analyzed. It was observed that a larger learning rate η accelerates the initial parameter convergence but can induce high-frequency oscillations in the tuned PID gains during steady-state phases. Conversely, an excessively small learning rate leads to sluggish parameter adaptation during rapid load mutations. The inertial coefficient α serves to smooth the weight updates; a moderate value of $\alpha = 0.05$ successfully balances the tracking speed and the smoothness of the control commands, minimizing chattering under noise-perturbed conditions.

4.5. Analysis of Comprehensive Evaluation Metrics for Control Performance

To further quantitatively evaluate the tracking accuracy and dynamic robustness of different control algorithms, this paper introduces four objective evaluation metrics: Root Mean Square Error (RMSE), Mean Absolute Error (MAE), Integral of Absolute Error (IAE), and Coefficient of Determination (R2) to conduct statistical analysis on the simulation data.

Data Analysis and Conclusion:

From the quantitative analysis results of Table 1, it can be seen that the global tracking accuracy of the traditional fixed parameter PID controller is the worst in the face of complex pipe network resistance mutations of coaxial water supply pump systems. Due to its inability to adapt to nonlinear load migration in real time, it produces a large number

of adjustment lags and overruns, resulting in its absolute error integral (IAE) as high as 12,380.1184. Although conventional sliding mode control (SMC) has strong nonlinear anti-interference ability, reducing the mean square root error (RMSE) and absolute error integral to 0.9966 and 5936.3966, respectively, it is limited by its convergence characteristics, and there are still obvious local residual deviations.

Table 1. Comparison of comprehensive performance metrics of different control algorithms under variable load jump conditions.

Evaluation Metric	Traditional PID	Traditional SMC	Improved BP-PID
RMSE	1.6126	0.9966	0.1888
MAE	1.2380	0.3958	0.0774
IAE	12,380.1184	5936.3966	774.0313
ISE	31,806.4458	14,897.8258	411.8516
ITAE	87,040,536.65	41,193,054.44	5,423,155.81
R^2	0.9885	0.9943	0.9998

In contrast, the improved BP-PID algorithm proposed in this study demonstrates enhanced tracking accuracy and robust performance. Through the adaptive weight adjustment and anti-integration saturation logic of the neural network, this algorithm reduced the Root Mean Square Error (RMSE) by 88.29% (0.1888) compared with the traditional PID, while the average absolute error (MAE) and cumulative error were reduced by 93.75%. Additionally, the fit of the improved algorithm (R^2) reached 0.999843, approaching the ideal value of 1.

This set of rigid indicators fully proves that the control strategy proposed in this paper can perfectly capture the complex nonlinear trend of actual working conditions, with high steady-state accuracy and dynamic tracking ability, and meet the strict requirements of high servo accuracy for the domestic transformation of water control of large thermal power units.

4.6. Computational Complexity Analysis

To further evaluate the feasibility of real-world deployment on embedded platforms or industrial Distributed Control Systems, it is necessary to assess the computational complexity of the proposed algorithm. Following the methodology proposed in the recent literature [20], the Simulink Profiler tool was utilized to record and analyze the execution overhead of different controllers during the 18,000-s simulation. The computational performance metrics, including Total Recorded Time, Number of Calls, and Time per Call, are summarized in Table 2.

Table 2. Computational complexity analysis of different control algorithms using Simulink Profiler.

Controller Module	Number of Calls	Total Recorded Time (s)	Self Time (s)	Time per Call (μs)
Traditional PID	200,013	5.718	0.225	0.12
Conventional SMC	200,013	3.576	0.261	1.30
Improved BP-PID	200,013	4.480	1.845	9.22

Data Analysis and Conclusion:

As shown in Table 2, the Traditional PID and Conventional SMC exhibit extremely low computational complexity, with their self-execution time per call being approximately

1.12 μs and 1.30 μs, respectively, owing to their simple linear or algebraic switching structures. In contrast, the proposed Improved BP-PID algorithm naturally demands additional computational overhead due to the continuous forward mapping of the three-layer neural network and the backpropagation weight updating matrices. Consequently, its "Self Time" per call increases to approximately 9.22 μs.

However, from a practical deployment perspective, modern industrial Distributed Control Systems or embedded microcontrollers typically operate on control cycles ranging from 10 ms to 50 ms. The 9.22 μs computational delay incurred by the proposed algorithm consumes less than 0.1% of a standard industrial control cycle. Therefore, it is definitively proven that the increased computational complexity of the Improved BP-PID is negligible in real-world scenarios. The algorithm perfectly meets the hard real-time execution constraints of embedded platforms, providing a highly feasible solution for the localization transformation of power plant control systems.

5. Conclusions

Aiming at the nonlinear and time-varying characteristics of the turbine-driven coaxial boiler feed pump (TD-BFP) system, this paper proposes an improved BP-PID control method introducing sign-preserving mapping, anti-integral windup, and first-order inertial filtering. By building a detailed fluid-mechanical coupled mathematical model and conducting simulation experiments, the following conclusions are drawn:

The traditional square term model will destroy the transmission of the negative control gradient. The $u|u|$ mapping adopted in this paper effectively solves the unidirectional out-of-control problem in nonlinear systems.

When facing high-frequency step conditions at 3683 RPM, the improved algorithm exhibits extremely high robustness, successfully overcoming local learning stagnation and high-frequency oscillation.

The model possesses high fidelity and can accurately fit the actual operation data of power plants, providing solid theoretical support and a simulation platform for the digital twin pre-simulation and parameter optimization of subsequent thermal power unit control strategies.

Future research will focus on transitioning the proposed control framework from the digital twin simulation environment to physical verification. Specifically, we plan to implement hardware-in-the-loop testing and subsequent real-world physical site deployment on the target steam turbine coaxial feedwater pump system. This physical validation will allow us to evaluate the controller's long-term operational reliability, robustness against physical actuator degradation, and adaptability under complex field-noise conditions in actual power plants.

Author Contributions: Conceptualization, N.M. and L.Y.; methodology, N.M. and Z.Y.; software, L.L.; validation, L.L. and L.W.; formal analysis, N.M. and Y.T.; investigation, L.L. and B.F.; resources, B.F.; data curation, N.M. and Y.T.; writing—original draft preparation, N.M.; writing—review and editing, L.W. and Z.Y.; visualization, Y.T.; supervision, L.Y.; project administration, L.Y.; funding acquisition, L.Y. All authors have read and agreed to the published version of the manuscript.

Funding: This Research is Supported by the Technology Project of the State Grid North China Electric Power Research Institute: Research on Localization Modification of Speed Control System for the First Domestic Steam Turbine Coaxial Feedwater Pump (Project Number: KJZ2025074).

Data Availability Statement: The original contributions presented in this study are included in the article. Further inquiries can be directed to the corresponding author.

Conflicts of Interest: Authors Ning Ma, Lei Liu, and Zhenyong Yang were employed by the company North China Electric Power Research Institute Co., Ltd.; Authors Bin Feng and Li Wang were employed by the company Xi'an Branch of North China Electric Power Research Institute Co., Ltd. The remaining authors declare that the research was conducted in the absence of any commercial or financial relationships that could be construed as a potential conflict of interest.

Abbreviations

The following abbreviations are used in this manuscript:

BIBO	Bounded-Input–Bounded-Output
BP	Back Propagation
BP-PID	Back Propagation—Proportional–Integral–Derivative
FLC	Fuzzy Logic Control
HOSMC	Higher-Order Sliding Mode Control
IAE	Integral of Absolute Error
ISE	Integral Square Error
ITAE	Integral of Time-weighted Absolute Error
MAE	Mean Absolute Error
NN	Artificial Neural Network
PID	Proportional–Integral–Derivative
RMSE	Root Mean Square Error
SMC	Sliding Mode Control
TD-BFP	Turbine-Driven Coaxial Boiler Feed Pump

References

1. Deng, K.; Yang, C.; Chen, H.; Zhou, N.; Huang, S. Start-Up and dynamic processes simulation of supercritical once-through boiler. *Appl. Therm. Eng.* **2017**, *115*, 937–946. [CrossRef]
2. Astrom, K.J.; Bell, R.D. Drum-boiler dynamics. *Automatica* **2000**, *36*, 363–378. [CrossRef]
3. Borase, A.; Maghade, D.K.; Sondkar, S.Y.; Pawar, S.N. A review of PID control, tuning methods and applications. *Int. J. Dyn. Control.* **2021**, *9*, 818–827. [CrossRef]
4. Bohn, C.; Atherton, D.P. An analysis package comparing PID anti-windup strategies. *IEEE Control. Syst. Mag.* **1995**, *15*, 34–40.
5. Wu, L.; Liu, J.; Vazquez, S.; Mazumder, S.K. Sliding mode control in power converters and drives: A review. *IEEE/CAA J. Autom. Sin.* **2021**, *9*, 392–406. [CrossRef]
6. Utkin, V.; Poznyak, A.; Orlov, Y.; Polyakov, A. Conventional and high order sliding mode control. *J. Frankl. Inst.* **2020**, *357*, 10244–10261. [CrossRef]
7. Levant, A. Sliding order and sliding accuracy in sliding mode control. *Int. J. Control.* **1993**, *58*, 1247–1263. [CrossRef]
8. Chalanga, A.; Kamal, S.; Fridman, L.M.; Bandyopadhyay, B.; Moreno, J.A. Implementation of super-twisting control: Super-twisting and higher order sliding-mode observer-based approaches. *IEEE Trans. Ind. Electron.* **2016**, *63*, 3677–3685. [CrossRef]
9. Ding, S.; Zheng, W.X.; Sun, J. A review on continuous-time sliding mode control. *Int. J. Syst. Sci.* **2018**, *49*, 3304–3315.
10. Landau, I.D.; Lozano, R.; M'Saad, M.; Karimi, A. *Adaptive Control: Algorithms, Analysis and Applications*; Springer Science & Business Media: New York, NY, USA, 2011.
11. Li, X.; Zhang, W. Coordinated Control of Circulating Fluidized Bed Boiler Based on the Fuzzy PID Control. In *2012 Annual Meeting of the North American Fuzzy Information Processing Society (NAFIPS), Berkeley, CA, USA, 6–8 August 2012*; IEEE: New York, NY, USA, 2012; pp. 16–22.
12. Naoual, R.; Mellouli, E.M.; Boumhidi, I. Adaptive fuzzy sliding mode control for the two-link robot. In *Proceedings of the 2014 9th International Conference on Intelligent Systems: Theories and Applications (SITA)*; IEEE: New York, NY, USA, 2014; pp. 1–6.
13. Kong, L.; Gu, R.; Wang, Q.; Ju, X.; Ding, W. Fuzzy Model Predictive Tracking Control for Boiler-Turbine Systems with Disturbances and Input Constraints. *Mathematics* **2025**, *23*, 3755. [CrossRef]
14. Deng, W.; Yao, J.; Ma, D. Robust adaptive precision motion control of hydraulic actuators with valve dead-zone compensation. *ISA Trans.* **2017**, *70*, 269–278. [CrossRef] [PubMed]
15. Yang, Z.; Gu, Y.; Bian, J. Analysis of Internal Leakage in Multistage Centrifugal Pumps under Conditions of Impeller Oscillation and Non-oscillation. *J. Phys. Conf. Ser.* **2024**, *2854*, 012019. [CrossRef]
16. Omatu, S.; Khalid, M.; Yusof, R. *Neuro-Control and Its Applications*; Springer Science & Business Media: New York, NY, USA, 2012.

17. Shahraki, F.; Fanaei, M.A.; Arjomandzadeh, A.R. Adaptive system control with PID neural networks. *Chem. Eng. Trans.* **2009**, *17*, 1395–1401.
18. Cong, S.; Liang, Y. PID-like neural network nonlinear adaptive control for uncertain multivariable motion control systems. *IEEE Trans. Ind. Electron.* **2009**, *56*, 3872–3879. [CrossRef]
19. *IEC 61131-3*; Programmable Controllers—Part 3: Programming Languages. International Electrotechnical Commission (IEC): Geneva, Switzerland, 2013.
20. Silaa, M.Y.; Barambones, O.; Bencherif, A. A novel adaptive PID controller design for a PEM fuel cell using stochastic gradient descent with momentum enhanced by whale optimizer. *Electronics* **2022**, *11*, 2610. [CrossRef]

Disclaimer/Publisher's Note: The statements, opinions and data contained in all publications are solely those of the individual author(s) and contributor(s) and not of MDPI and/or the editor(s). MDPI and/or the editor(s) disclaim responsibility for any injury to people or property resulting from any ideas, methods, instructions or products referred to in the content.